

#### **ARTICLE**



1

https://doi.org/10.1038/s41467-022-30421-5

**OPFN** 

# Subducted organic matter buffered by marine carbonate rules the carbon isotopic signature of arc emissions

Ocean sediments consist mainly of calcium carbonate and organic matter (phytoplankton debris). Once subducted, some carbon is removed from the slab and returns to the atmosphere as  $CO_2$  in arc magmas. Its isotopic signature is thought to reflect the bulk fraction of inorganic (carbonate) and organic (graphitic) carbon in the sedimentary source. Here we challenge this assumption by experimentally investigating model sediments composed of  $^{13}C$ - $CaCO_3 + ^{12}C$ -graphite interacting with water at pressure, temperature and redox conditions of an average slab-mantle interface beneath arcs. We show that oxidative dissolution of graphite is the main process controlling the production of  $CO_2$ , and its isotopic composition reflects the  $CO_2/CaCO_3$  rather than the bulk graphite/ $CaCO_3$  (i.e., organic/inorganic carbon) fraction. We provide a mathematical model to relate the arc  $CO_2$  isotopic signature with the fluid-rock ratios and the redox state in force in its subarc source.

<sup>&</sup>lt;sup>1</sup> Dipartimento di Scienze della Terra, Università degli Studi di Milano, via Mangiagalli 34, I-20133 Milano, Italy. <sup>2</sup> Dipartimento di Scienza e Alta Tecnologia, Università degli Studi dell'Insubria, via Valleggio 11, I-22100 Como, Italy. <sup>3</sup> Institut de Minéralogie, de Physique des Matériaux, et de Cosmochimie (IMPMC), Sorbonne Universités – UPMC, UMR CNRS, 7590, Muséum National d'Histoire Naturelle, IRD UMR 206, F-75005 Paris, France. <sup>4</sup> Institut für Mineralogie, Universität Münster, Correnstrasse 24, 48149 Münster, Germany. <sup>5</sup> Department of Earth & Planetary Sciences, Johns Hopkins University, Baltimore, MD 21218, USA. <sup>6</sup> Department of Earth, Planetary and Space Sciences, University of California, Los Angeles, CA 90095-1567, USA. <sup>7</sup> Dipartimento di Scienze Biologiche, Geologiche e Ambientali (BiGeA), Alma Mater Studiorum Università di Bologna, 40126 Bologna, Italy. <sup>8</sup> Dipartimento di Scienze della Terra, Università degli Studi di Torino, via Valperga Caluso 35, 10125 Torino, Italy. <sup>80</sup> email: simone.tumiati@unimi.it

odern open-ocean sediments are dominated by phytoplankton. Calcium carbonate, chiefly in sediments deposited above the calcite compensation depth, is essentially calcite forming the shells of organisms such as coccolithophores. It displays carbon isotopic ratios comparable to bicarbonate ions dissolved in seawater, characterized by  $\delta^{13}$ C  $\approx 0\%$  expressed as  $^{13}$ C/ $^{12}$ C per mil difference normalized to the international Vienna-Pee Dee Belemnite (VPDB) standard. Conversely organic matter, which is essentially phytoplankton debris in the open seafloor, is depleted at <sup>13</sup>C due to fractionation effects induced by photosynthesis, such that  $\delta^{13}C \approx -20\%$ VPDB<sup>1</sup>. Stable carbon isotopes and mass-balance calculations relying on simple mixing models have been used extensively to determine the relative contribution of organic matter and marine carbonates in sedimentary rocks<sup>2</sup>, in their metamorphic equivalents<sup>3</sup> and in volcanic arc emissions<sup>4</sup>. However, the applicability of simple mixing models hinges on assumptions that may be overly simplistic, including that the sedimentary "endmember" compositions are spatially and temporally invariant, and that isotopic equilibrium is attained during metamorphism. The latter is particularly problematic because sedimentary organic carbon and coexisting carbonate may exhibit substantial isotopic exchange with increasing metamorphic grade, in particular at temperatures >650 °C during prograde graphitization<sup>3,5-7</sup>. In turn, fully crystalline graphite displays a sluggish rate of isotopic diffusion and may be unaffected by isotopic reset even in cases of Q1 –Q5 intense metamorphism and fluid/rock interactions8.

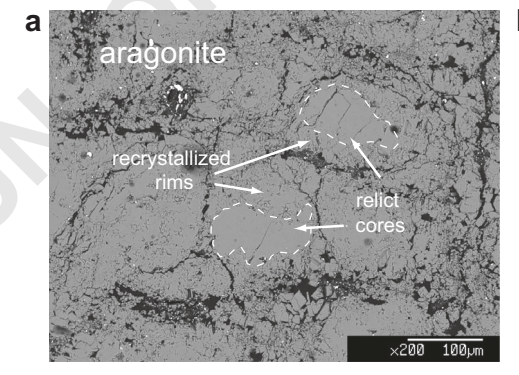
Carbonates and graphitic carbon derived from organic matter, formerly assumed to be refractory to dissolution and devolatilization during subduction<sup>9,10</sup>, are now thought to show a nonnegligible solubility in subduction fluids at least at certain  $P-T-fO_2$ -pH conditions<sup>11-18</sup>. The interaction of subducted sediments with deep fluids<sup>14,19</sup> produces dissolved carbon that is transferred from the slab to the overlying mantle wedge, prompting carbonation/metasomatism and/or partial melting $^{20-23}$ , and eventually returning to the surface via  $CO_2$ emitted by arc volcanoes<sup>4</sup>. The global arc average  $\delta^{13}$ C is -2.8 to -3.3 %. This is heavier than the major carbon isotopic composition signature of the upper mantle  $(\delta^{13}C = -6.0 \pm 2.5\%)^4$ , but significantly lighter than sedimentary carbonates  $(\delta^{13}C \approx 0\%^{24})$ . As it is generally assumed that the carbon isotope signature of arc emissions reflects that of their source, relatively high  $\delta^{13}$ C values would point out assimilation of shallow "crustal" limestones, while low  $\delta^{13}$ C are usually attributed to subducted organic carbon<sup>4</sup>. However, processes of dissolution and of isotopic exchange involving organic and inorganic carbon beneath arcs are still not fully understood.

In this work, we investigate the carbon isotopic exchange occurring in a model system representative of open-ocean sediments containing calcium carbonate + organic matter subducted at subarc depths and interacting with aqueous fluids rising from the underlying dehydrating oceanic lithosphere<sup>25</sup>. We provide the quantitative chemical analysis of the volatile species and the measured carbon isotopic composition of CO<sub>2</sub> produced by dissolution in water of graphite and of aragonite at P = 3 GPa,  $T = 700 \,^{\circ}\text{C}$  and at redox-controlled conditions buffered to  $\Delta FMQ = +0.61 \log \text{ units}$ . These conditions are selected on the basis of the predicted peak of CO<sub>2</sub> produced by oxidative dissolution of graphite in subduction zones (Supplementary Fig. 1). Starting materials of synthetic labelled CaCO<sub>3</sub> (99.4% <sup>13</sup>C) and synthetic graphite (98.9% <sup>12</sup>C) are used as analogues for natural "heavy" carbonate and "light" organic matter and to generate a maximum isotopic difference in experiments (close to pure <sup>13</sup>C and <sup>12</sup>C end-members). Control experiments are performed with oxalic acid di-hydrate (98.7% <sup>12</sup>C) as the source of CO<sub>2</sub> instead of graphite. The dissolution process and the effect of different CO<sub>2</sub>/ aragonite ratios and of different run durations from 0.24 to 240 h are evaluated and compared with thermodynamic calculations that include consideration of aqueous solute speciation<sup>26–28</sup> or consider only gas speciation in a conventional graphite-saturated COH fluid model<sup>29,30</sup>. Finally, a comparison with conventional isotopic models is provided. Experimental data allow the development of mathematical models extending the applicability of the results to a wide range of redox conditions and of fluid/rock ratios in order to predict the  $\delta^{13}$ C of CO<sub>2</sub> released from the sedimentary slab and to envisage conditions required to meet the global average arc signature.

#### **Results and discussion**

CO<sub>2</sub> evolved by the aqueous dissolution of aragonite-only, graphite-only and mixed aragonite + graphite. In all experiments we observed that aragonite crystals in run products displayed textural evidence of dissolution-reprecipitation, including step edges, and fine-grained recrystallized rims around larger relict cores (Fig. 1). Conversely, we never observed texturally precipitation of newly formed graphite or graphite recrystallization, nor evidence for graphite isotopic variation compared to its starting composition.

In aragonite-only runs, despite the evidence of dissolution–precipitation microtextures, the absolute amount of  $CO_2$  evolved by the aqueous dissolution of aragonite-only is very low, close to the analytical detection limit, with  $XCO_2$  [ =  $CO_{2(aq)}/(H_2O + CO_{2(aq)})_{molar}$ ] = 0.001 corresponding to 0.041 mol  $CO_2/kg$   $H_2O$  (Fig. 2a; Supplementary Tables 1 and 2). We compared this result with thermodynamic modelling performed at the investigated



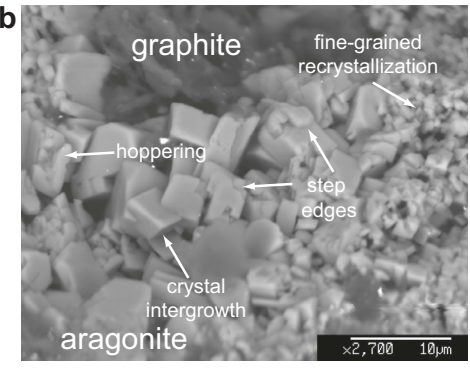


**Fig. 1 Electron microscope images showing microtextures of run products. a** Recrystallized aragonite, showing rims of sub-micrometric crystals surrounding relict cores 50–100 μm in size. **b** Assemblage graphite + aragonite; aragonite crystals show dissolution/reprecipitation microtextures such as crystal size reduction, hoppering, step edges and euhedral crystal intergrowth.

2

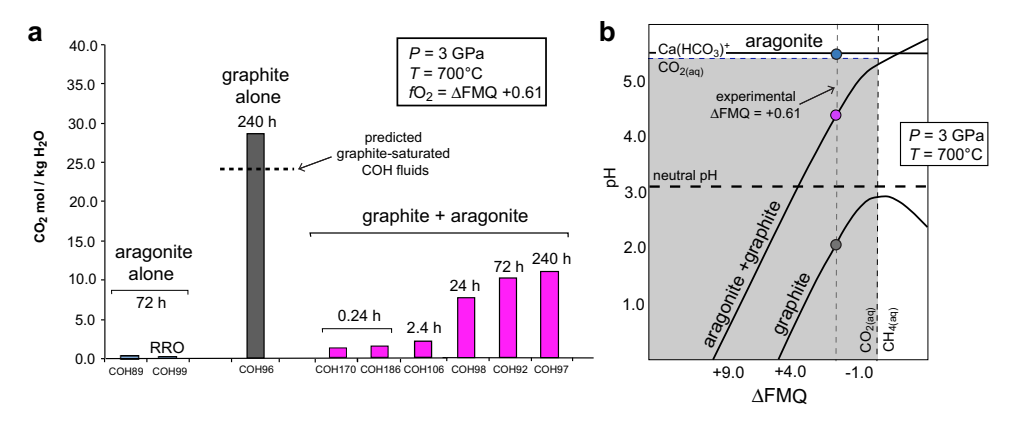


**Fig. 2 Experimental CO<sub>2</sub> contents and thermodynamic modelling of fluids.** Calculations are performed at 3 GPa, 700 °C and  $fO_2$  buffered by ferrosilite + magnetite + coesite + H<sub>2</sub>O (log  $fO_2 = -13.36$ ; ΔFMQ = +0.61). **a** CO<sub>2</sub> concentration (molality) in aqueous fluid interacting with (i) aragonite-only (blue), (ii) graphite-only (grey) and (iii) graphite + aragonite (magenta). Typical analytical uncertainty is 1%. Dashed line: CO<sub>2</sub> content predicted by thermodynamic modelling of graphite-saturated COH fluids. Run duration (h) is shown at the top of each bar. RRO: run buffered by Re-ReO<sub>2</sub> (ΔFMQ ≈ +2) instead of ferrosilite + magnetite + coesite; **b**  $fO_2$  vs. pH diagram at 3 GPa and 700 °C generated by thermodynamic modelling (Deep Earth Water model<sup>26,28</sup>) of aqueous fluids in equilibrium with aragonite-only (blue dot), graphite-only (grey dot) and aragonite + graphite (magenta dot). Black solid lines: saturation curves. Coloured dots: experimental conditions at  $fO_2$  buffered by ferrosilite + magnetite + coesite. Grey field: CO<sub>2(aq)</sub> is the dominant carbon-bearing species; it is adjacent to Ca(HCO<sub>3</sub>)+-dominated field at higher pH and to CH<sub>4(aq)</sub>-dominated field at lower  $fO_2$  values. Neutral pH is shown for reference with a dashed line.

 $P-T-fO_2$  conditions using the Deep Earth Water (DEW) model<sup>26,28</sup> (Fig. 2b; Supplementary Table 3). Calculations indicate that fluids in equilibrium with pure aragonite should display a basic pH = 5.09 (neutral pH = 3.09 at 3 GPa and 700 °C) and  $XCO_2 = 0.0002$ , which is even lower than the measured value. However, the model predicts that the dominant carbon-bearing dissolution product of aragonite at the investigated conditions is the calcium-bicarbonate ion Ca(HCO<sub>3</sub>)<sup>+</sup>, in agreement with previous studies <sup>13,14</sup>. According to the model, a substantial concentration of carbon is present in the form of ionic species. In particular, Ca(HCO<sub>3</sub>)<sup>+</sup> accounts for the 74.3 mol% of the total carbon-bearing dissolved species, while CO<sub>2(aq)</sub> only 7.3 mol% (Supplementary Table 3). The solubility of aragonite is therefore higher than that inferred on the basis of the measured CO<sub>2</sub> only. As Ca(HCO<sub>3</sub>)<sup>+</sup> is not measurable by QMS, we rely on the predicted Ca(HCO<sub>3</sub>)<sup>+</sup> abundance to correct up the bulk aragonite solubility to 0.459 mol CO<sub>2</sub>/kg H<sub>2</sub>O, equivalent to  $5.28 \times 10^3$  ppm (=mg C/kg solution; 495 ppm of which deriving from measured  $CO_{2(aq)}$ ), which agrees well with previous estimates<sup>14</sup>. In aragonite-only runs, the evolved CO<sub>2</sub> is independent of  $fO_2$ , as demonstrated by the nearly identical  $XCO_2 = 0.002$  in the more oxidized ( $\approx \Delta FMQ + 2$ ) control run buffered by Re-ReO<sub>2</sub> (RRO in Fig. 2a; Supplementary Tables 1 and 2). On the contrary, the addition of ~0.5 molal to ~1 molal chlorine to lower pH in control experiments effectively boosts fluid CO<sub>2</sub> concentrations to  $2.17-2.46 \text{ mol CO}_2/\text{kg H}_2\text{O}$  (corresponding to  $XCO_2 = 0.038-0.042$ ; Supplementary Tables 1 and 2).

Compared to runs with aragonite-only, the  $CO_2$  amount in fluids in experiments with graphite-only is significantly higher, with  $XCO_2=0.339$  after 240 h (Fig. 2a) corresponding to 28.5 mol  $CO_2$ /kg  $H_2O$  and a carbon concentration of  $1.52\times10^5$  ppm, two orders of magnitude higher than in fluids dissolving aragonite-only (Fig. 2a; Supplementary Tables 1 and 2). DEW model calculations show that fluids in equilibrium with pure graphite should display an acidic pH = 2.21 (Fig. 2b) and  $XCO_2=0.305$  (Supplementary Table 3), which is nearly identical to the value of  $XCO_2=0.303$  predicted by conventional modelling of graphite-saturated COH fluids<sup>29–31</sup> (Fig. 2a; Supplementary Table 4) and close to the measured value of 0.339. In fluids in equilibrium with graphite-only,  $CO_{2(aq)}$  is predicted to account for 99.93% of the total dissolved carbon (Supplementary Table 3).

The CO<sub>2</sub> amount measured in time-resolved runs containing mixed aragonite and graphite (Fig. 2a; Tables 1 and 2) ranges from  $XCO_2 = 0.026$  after 0.24 h to 0.166 after 240 h. Results suggest that chemical equilibrium is almost reached after 72 h. After 240 h, fluids contain 11.19 mol CO<sub>2</sub>/kg<sub>water</sub> corresponding to  $8.96 \times 10^4$  ppm C, about one half that in fluids in equilibrium with graphite-only. This decline is not anticipated by either the DEW model calculations-which predict only a slightly lower XCO<sub>2</sub> of 0.284 for fluids in equilibrium with graphite-only (Supplementary Table 3)—or by the graphite-saturated COH fluid model-which cannot account for the dissolution of aragonite because it does not consider components other than C, O and H. Our experimental result confirms that the estimation of XCO<sub>2</sub> with available thermodynamic models is hampered in complex systems<sup>15</sup>. Nevertheless the DEW model is still useful to predict that fluids in equilibrium with both aragonite and graphite display a basic pH = 4.2 (Supplementary Table 3), which is higher than fluids in equilibrium with graphite-only but lower than fluids in equilibrium with aragonite-only, dominated by the dissolution product Ca(HCO<sub>3</sub>)<sup>+</sup> (Fig. 2b). The consequence is that, as in fluids in equilibrium with graphite alone,  $CO_{2(aq)}$  is calculated to predominate in fluids in equilibrium with both graphite and aragonite (Fig. 2b), with CO<sub>2(aq)</sub> accounting for 91.4% of the total carbon-bearing species, whereas Ca(HCO<sub>3</sub>)<sup>+</sup> constitutes only 3.70% of the total carbon in solution (Supplementary Table 3).

# Carbon isotopic composition of graphite, aragonite and $\rm CO_2$ . In experiments where water interacts with single minerals, the isotopic abundances of evolved $\rm CO_2$ are identical to that of the starting materials within analytical uncertainties. In particular, due to the analytical sensitivity of QMS, this is evident in runs characterized by higher $\rm CO_2$ production, i.e. $\rm ^{13}C$ -aragonite + chlorine and $\rm ^{12}C$ -graphite-only runs. In graphite-alone runs, the average $\rm CO_2$ isotopic abundance is 1.11% $\rm ^{13}C$ after 240 h (Supplementary Table 1), indistinguishable from the $\rm ^{13}C$ abundance of the starting graphite (1.09% $\rm ^{13}C$ measured by IRMS; Supplementary Fig. 2) considering analytical uncertainties.

The isotopic signature of evolved  $CO_2$  in experiments with both  $^{13}$ C-aragonite and  $^{12}$ C-graphite (Fig. 3a; Supplementary Table 1) is relatively rich in  $^{12}$ C ( $^{13}$ C = 52.9–62.8%) only in runs

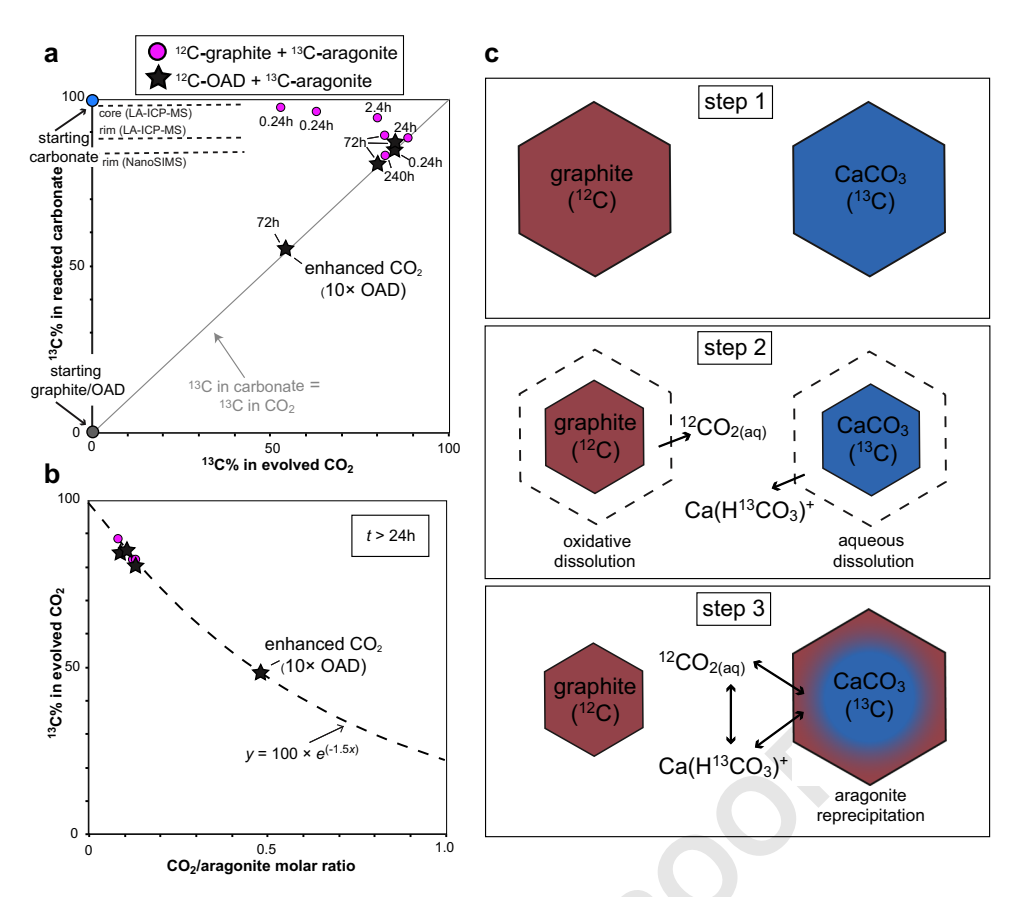


**Fig. 3 Isotopic composition of experimental fluids and solids. a** Measured  $^{13}$ C abundance (%) in CO<sub>2</sub> versus bulk after-run aragonite. Grey reference line indicates identical  $^{13}$ C abundances in CO<sub>2</sub> and in bulk aragonite. Magenta dots:  $^{13}$ C-CaCO<sub>3</sub> + graphite runs. Starting  $^{13}$ C% of carbonate and graphite are indicated with blue and grey dots, respectively. Representative point analyses of aragonite cores and rims are shown with black dashed lines. Black stars: oxalic acid di-hydrate (OAD; starting  $^{13}$ C% is coincident with starting graphite) +  $^{13}$ C-CaCO<sub>3</sub> runs. **b** CO<sub>2</sub>/ $^{13}$ C-CaCO<sub>3</sub> molar ratio plotted against  $^{13}$ C abundance (%) in CO<sub>2</sub> of runs with duration >24 h. Dashed line represents the best fit of the data using an exponential equation. **c** Conceptual model for the carbon isotope exchange observed in experiments. At step 1, isotopically pure  $^{12}$ C-graphite (brown) and  $^{13}$ C-aragonite (blue) coexist in the same assemblage. As the interaction with water starts (step 2), graphite undergoes oxidative dissolution forming  $^{12}$ CO<sub>2(aq)</sub>, while aragonite dissolves forming Ca(H $^{13}$ CO<sub>3</sub>)+, as predicted by thermodynamic modelling. While graphite oxidative dissolution is self-limiting because the maximum amount of CO<sub>2(aq)</sub>, in the fluid is constrained by the redox state of the system, aragonite undergoes a continuous process of dissolution/precipitation (step 3). Therefore, the final isotopic composition of CO<sub>2(aq)</sub>, which is in dynamic equilibrium with Ca(HCO<sub>3</sub>)+ and thus with aragonite, becomes rapidly enriched in  $^{13}$ C ending with  $^{13}$ C abundances of >80% of the starting  $^{13}$ C-aragonite.

characterized by a very short duration of 0.24 h, while it becomes relatively homogeneous for  $t \ge 24 \text{ h}$ reaching abundance = 82.2% after 240 h. Bulk measurements by means of total carbonate HCl dissolution allowed retrieval of the final average isotopic composition of after-run aragonite coexisting with CO<sub>2</sub> (y-axis in Fig. 3a; Supplementary Table 1). Low <sup>13</sup>C abundances in evolved CO<sub>2</sub> are always coupled with high <sup>13</sup>C in bulk aragonite, the latter tending to the starting <sup>13</sup>C-CaCO<sub>3</sub> value of 99.4% <sup>13</sup>C (blue dot in Fig. 3a) in the shortest 0.24 h  $(^{13}C = 96.1-97.2\%)$  and 2.4 h  $(^{13}C = 95.8\%)$  runs (Fig. 3a; Supplementary Table 1). In longer  $t \ge 24 \text{ h}$  runs, <sup>13</sup>C abundances of CO2 and of bulk carbonate converge (cf. black dashed line in Fig. 3a). After 240 h, the <sup>13</sup>C abundance in aragonite is 82.9%, nearly identical to that of evolved CO<sub>2</sub> (i.e. 82.2%).

Micro-analyses performed by means of NanoSIMS and LA-ICP-MS (dashed lines in Fig. 3a; Supplementary Tables 5 and 6) show that aragonite crystals are isotopically zoned, in particular in short runs, with recrystallized rims characterized by  $^{13}$ C abundances comparable to that of bulk aragonite and of CO<sub>2</sub> in longer runs (e.g.  $^{13}$ C = 81.6(8)% in the 24 h run COH106; Supplementary Table 6), and relict cores showing high  $^{13}$ C abundance up to 98(1)%  $^{13}$ C (e.g. run COH97; Supplementary

Table 6) approaching the starting composition of  $^{13}$ C-CaCO<sub>3</sub>. Conversely, the  $^{13}$ C abundance in after-run graphite indicates negligible isotopic re-equilibration (Supplementary Fig. 2; Supplementary Table 5, 6). NanoSIMS measurements range from 1.132(6)% to 1.195(3)% (Supplementary Fig. 2; Supplementary Table 5), concordant with LA-ICP-MS measurements ranging from  $^{13}$ C = 1.1(1)% to 1.5(2)% (Supplementary Fig. 2; Supplementary Table 6).

The  $^{12}$ C-rich composition of CO<sub>2</sub> in the shortest runs and the lack of newly formed graphite suggest that in mixed aragonite–graphite runs, the early source of CO<sub>2</sub> was graphite undergoing irreversible oxidation. To validate this hypothesis, we performed a series of control experiments at identical experimental conditions but without graphite, where the early source of  $^{12}$ CO<sub>2</sub> is provided by oxalic acid di-hydrate ( $^{13}$ C = 1.29%; OAD and black stars in Fig. 3a), which decomposes already at  $T \approx 200$  °C to a mixed  $H_2$ O-CO<sub>2</sub> fluid $^{32}$ . OAD has been added in the proper amount to keep the same CO<sub>2</sub>/ $^{13}$ C-CaCO<sub>3</sub> ratio  $\approx$  0.1 characterizing graphite + aragonite experiments (Fig. 3b; Supplementary Table 1). In addition, 10 times more OAD was added in a single run to increase the CO<sub>2</sub>/ $^{13}$ C-CaCO<sub>3</sub> ratio to a value of ~0.5 ("enhanced CO<sub>2</sub>" in Fig. 3a, b; Supplementary

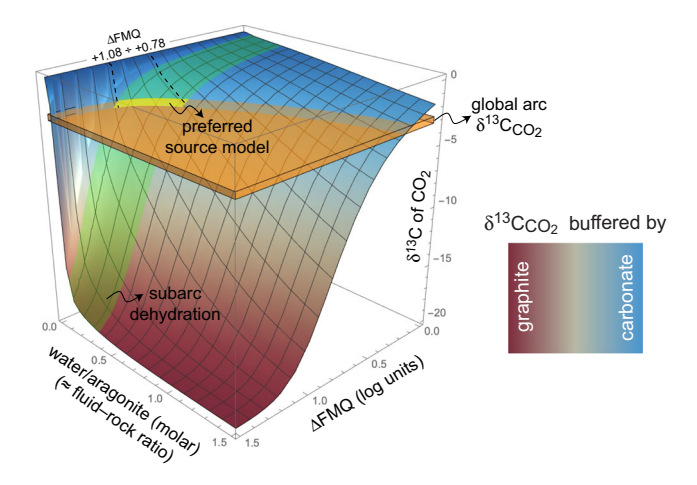


Fig. 4 Mathematical model showing the predicted  $\delta^{13}$ C of CO<sub>2</sub> as a function of both  $\Delta$ FMQ and water/aragonite ( $\approx$  fluid-rock) molar ratio.

Modelled  $CO_2$  is originated from oxidative dissolution of graphite and interacts with aragonite and aqueous fluids at 3 GPa and 700 °C. Brown surface color:  $\delta^{13}C$  buffered by graphite. Blue surface color:  $\delta^{13}C$  buffered by aragonite. Orange box: global average  $\delta^{13}C$  of arc  $CO_2^4$ ; the intersection with the mathematical model shows that arc  $CO_2$  signatures are met for a wide range of  $\Delta$ FMQ and fluid-rock ratios. Preferred model (yellow field) corresponds to the intersection among our mathematical model, the global average arc  $\delta^{13}C$  and typical fluid-rock ratios at slab-top conditions assuming percolating flux (green field; 0.05–0.33 molar = 0.01–0.06 mass). In this case,  $\Delta$ FMQ ranging from +0.78 to +1.08 are derived for the source of carbon in the sedimentary slab at subarc conditions.

Table 1). In OAD + <sup>13</sup>C-CaCO<sub>3</sub> runs with CO<sub>2</sub>/<sup>13</sup>C-CaCO<sub>3</sub> ratio ≈ 0.1, the isotopic composition of both CO<sub>2</sub> and bulk carbonate shows no appreciable differences compared to aragonite + graphite runs, further supporting the hypothesis of graphite as the early source of CO<sub>2</sub>. In addition, the OAD + <sup>13</sup>C-CaCO<sub>3</sub> run with CO<sub>2</sub>/<sup>13</sup>C-CaCO<sub>3</sub> ratio ≈ 0.5 makes evident that the <sup>13</sup>C abundance of CO<sub>2</sub> (and of coexisting aragonite) varies as a function of the CO<sub>2</sub>/<sup>13</sup>C-aragonite ratio (CAR), which can be described by the following exponential function (Fig. 3b):

$$^{13}C_{CO}\% = 100 \times e^{(-1.5 \times CAR)}$$
 (1)

which represents a mathematical model for the competing isotopic buffering in fluids where  $CO_2$  originated from the oxidative dissolution of  $^{12}\text{C}$ -graphite interacts with  $^{13}\text{C}$ -aragonite. Equation 1 shows that graphite-derived  $CO_2$  (and coexisting aragonite) are fully isotopically buffered by  $^{13}\text{C}$ -aragonite to  $^{13}\text{C}$  abundances  $\approx 100\%$  when CAR tends to zero. Conversely, by increasing CAR the contribution of  $^{12}\text{C}$ -graphite to the isotopic composition of  $CO_2$  becomes increasingly important, with  $^{13}\text{C}$  abundances tending to zero (i.e. fully buffered by graphite) at very high  $CO_2/^{13}\text{C}$ -aragonite ratios (e.g.  $^{13}\text{C}_{CO2}=0.01$  when CAR=6).

A conceptual model for carbon isotopic exchange among graphite, aragonite and  ${\rm CO_2}$ . In runs containing mixed  ${\rm ^{13}C}$ -aragonite and  ${\rm ^{12}C}$ -graphite, the isotopic composition of  ${\rm CO_2}$  after 24 h is nearly coincident with that of the recrystallized aragonite, although it is produced mainly by the oxidative dissolution of graphite which remains isotopically unchanged. Our experimental results confirm that carbon isotope exchange between graphite and aragonite at 700 °C is sluggish, in agreement with previous findings suggesting that carbon diffusion in graphite is very slow at  $T < 1300 \, ^{\circ}{\rm C}^{33,34}$ . In the shortest 0.24 h and 2.4 h runs, despite the similar  $^{13}{\rm C}$  abundances of  ${\rm CO_2}$  and

aragonite rims, the bulk carbonate <sup>13</sup>C is markedly higher because of a number of unreacted <sup>13</sup>C-rich cores persist, as shown by NanoSIMS and LA-ICP-MS analyses. In order to develop a conceptual model for the isotopic exchange among aragonite, graphite and CO<sub>2</sub>, we rely on observed microtextures, measurements and thermodynamic modelling results suggesting that during the run both graphite and aragonite undergo dissolution. However, <sup>12</sup>C-graphite produces mainly <sup>12</sup>CO<sub>2</sub> by irreversible oxidation, which can be expressed by the following *f*O<sub>2</sub>-dependent reaction:

$$^{12}C + O_2 = >^{12}CO_2$$
 (2)

 $^{13}$ C-aragonite dissolves initially forming mainly calciumbicarbonate ions (Ca( $H^{13}$ CO<sub>3</sub>) $^+$ ; Fig. 3c), according to the reactions involving the predominant species:

$$Ca^{13}CO_3H_2O < = >Ca(H^{13}CO_3)^+ + OH^-$$
 (3)

When the fluid becomes saturated with respect to graphite,  $\mathrm{CO}_2$  production by graphite oxidation stops and the unreacted graphite remains chemically and isotopically inert, while aragonite continuously dissolves and reprecipitates in dynamic equilibrium with the dissolved aqueous carbon species  $\mathrm{CO}_2$  and  $\mathrm{Ca}(\mathrm{HCO}_3)^+$ , which in turn exchange carbon isotopes according to the following reaction:

$$^{12}\text{CO}_2 + \text{Ca}(\text{H}^{13}\text{CO}_3)^+ < = >^{13}\text{CO}_2 + \text{Ca}(\text{H}^{12}\text{CO}_3)^+$$
 (4)

Therefore, because of the continuous dissolution/reprecipitation process controlled by Eq. 3, the carbonate is effective in buffering the isotopic signature of  $\rm CO_2$  even after a very short time, despite the fact that  $\rm CO_2$  is produced mainly by irreversible oxidation of graphite. Equation 1, however, predicts that aragonite buffering is possible only for relatively low  $\rm CO_2/$  aragonite ratios, ideally below 0.46 where the  $^{13}\rm C$  abundances would be >50%. We will show below that Eq. 1 can be used to evaluate how the isotopic compositions of  $\rm CO_2$  evolved from the sedimentary slab at subarc conditions can meet the global average arc signature according to those variables that control the  $\rm CO_2$  release, i.e. the fluid/rock ratios and the redox conditions imposed by the environment.

A mathematical model for  $\delta^{13}$ C of CO<sub>2</sub> produced in the sedimentary slab and comparison with global average arcs. Thermodynamic considerations require that at graphite saturation and at fixed P-T conditions the amount of CO<sub>2</sub> produced by oxidation of graphite in a pure, carbonate-free C-O-H system depends solely on: (i) redox conditions—the more oxidizing they are, the higher the XCO<sub>2</sub> (=CO<sub>2,aq</sub>/(H<sub>2</sub>O+CO<sub>2,aq</sub>))<sup>35</sup>, and (ii) the amount (number of moles) of H<sub>2</sub>O interacting with graphite—the higher it is, the higher the amount of CO<sub>2</sub> at fixed XCO<sub>2</sub><sup>30,36</sup>. Therefore, at graphite saturation conditions and as long as graphite is present, the amount of CO<sub>2</sub> produced by oxidation is not dependent on the amount of graphite in the system.

In graphite + aragonite + H<sub>2</sub>O systems, we demonstrated that the carbon contribution to fluids due to aragonite dissolution is negligible at subarc P-T conditions compared to graphite, so the amount of CO<sub>2</sub> evolved still depends on (i) and (ii) above, with the additional consequence that the graphite/carbonate ratio is again not relevant. Moreover, the carbon content in these fluids is basically ascribable to their CO<sub>2</sub> content, as Ca(HCO<sub>3</sub>)<sup>+</sup> is limited to about 1%. However, we noticed a difference in the aragonite + graphite system compared to the graphite-alone (COH) system: the halving of measured XCO<sub>2</sub> (=0.166) compared to graphite-saturated COH fluid models (=0.303; Fig. 2a). By analogy with other systems, we suggest that this is likely related to a modification of water activity  $^{15}$ , in this case due to aragonite dissolution. Applying the experimentally derived

correction factor of 0.548 (=0.166/0.303), we calculated for the aragonite + graphite system the XCO<sub>2</sub> values predicted by conventional graphite-saturated fluid thermodynamic model<sup>29,30</sup> at different redox conditions ( $\Delta$ FMQ). The calculated  $XCO_2$  were used to calculate the absolute amount of CO2 produced by oxidation of graphite, obtained by fixing the absolute amount (moles) of H<sub>2</sub>O in the system. Assuming 1 mol aragonite in the system, fixed H<sub>2</sub>O values correspond also to water/aragonite molar ratios (WAR) and CO2 values to CO2/aragonite molar ratios. Using these last values and Eq. 1, we calculated the <sup>13</sup>C abundance of CO<sub>2</sub> produced by oxidation of <sup>12</sup>C-graphite after interaction with <sup>13</sup>C-aragonite. Because in our experimental model <sup>12</sup>C-graphite and <sup>13</sup>CaCO<sub>3</sub> represent analogues of, respectively, ocean organic matter with  $\delta^{13}$ C  $\approx -20$  and marine carbonates with  $\delta^{13}C \approx 0$ , we are now able to translate  $^{13}C$ abundances (ranging from 0 to 100%) to equivalent  $\delta^{13}$ C values (ranging from 0% to -20%) using a conventional linear model:

$$\delta^{13}C\% = 0.2 \times {}^{13}C\% - 20 \tag{5}$$

The calculated  $\delta^{13}$ C‰ of CO<sub>2</sub> repeated for 10,000 different random combinations of the parameters  $\Delta$ FMQ and WAR have been fitted with a three-variate parametric equation to provide, with an estimated average uncertainty of  $\pm 0.2\%$ , the following mathematical model (Fig. 4):

$$\delta^{13} C_{CO_2} \% = -20 + 20 \frac{1}{1 + e^{-f(\triangle FMQ, WAR)}}$$
 (6)

where the function  $f(\Delta FMQ, WAR)$  is a third-order polynomial found to minimize residuals (parameters and associated uncertainties available in Supplementary Table 7). The global arc  $\delta^{13}C$  ranging from -2.8 to -3.3 ‰<sup>4</sup> (orange box in Fig. 4) intersects the surface of Eq. 6 providing a continuous layer that can be averaged and expressed with the following equation:

$$\Delta \text{FMQ} = \frac{2}{1 + e^{(A+B \times \text{WAR} + C \times \text{WAR}^2 + D \times \text{WAR}^3)}}$$
 (7)

Equation 7, where A = -0.314(9), B = 2.75(5), C = -1.46(6) and D = 0.37(2), represents the locus of points of all the possible combinations of  $\Delta$ FMQ and water/aragonite ratio that result in the isotopic composition of sediment-derived  $CO_2$  satisfying the global average arc values.

Comparison with conventional mass-balance/equilibrium fractionation models. The observed carbon isotopic exchange among  $CO_2$ , graphite and aragonite is potential of interest for subducted sediments buried in a wide range of basins; the only limiting factor is the coexistence of calcium carbonate with elemental carbon (formerly organic matter) in whatever proportion and the presence of an aqueous fluid. Our experiments at 3 GPa and 700 °C show that  $CO_2$  produced by oxidative dissolution of  $^{12}C$ -graphite ( $^{13}C = 1.1\%$ ; equivalent  $\delta^{13}C = -19.8$ , cf. Eq. 5 and Supplementary Table 1) becomes rapidly enriched in  $^{13}C$  ending after 240 h with  $^{13}C = 82.2\%$  (equivalent  $\delta^{13}C = -3.56$ ) due to its isotopic exchange with  $^{13}C$ -aragonite ( $^{13}C = 99.6\%$ ; equivalent  $\delta^{13}C = -0.08$ ), despite the overwhelming abundance of graphite in the starting materials (graphite/aragonite<sub>(molar)</sub> = 5.6; see below).

Equivalent  $\delta^{13}C$  values can be compared with conventional models combining mass-balance calculations with isotope equilibrium fractionation (see Methods). Let's assume a mixture similar to what investigated experimentally: aragonite ( $\delta^{13}C=0\%$ , by analogy with a marine carbonate source) + graphite ( $\delta^{13}C=-20\%$ ; by analogy with a marine organic matter source), equilibrating at 700 °C (pressure effect ignored). Assuming complete solid–solid isotopic exchange and neglecting devolatilization, the final isotopic

composition would be a function of the molar ratio between graphite and aragonite, for instance: 1)  $\delta^{13}C_{graphite} = -5.29\%$ ;  $\delta^{13}C_{aragonite} = -0.14$  % for graphite/aragonite = 0.01; 2)  $\delta^{13}C_{graphite} = -12.57\%$ ;  $\delta^{13}C_{aragonite} = -7.43\%$  for graphite/aragonite = 1.0; 3)  $\delta^{13}C_{graphite} = -17.77\%$ ;  $\delta^{13}C_{aragonite} = -12.63\%$  for graphite/aragonite = 5.6. With the latter abundance value, comparable with the experimental setup, calculations show that the isotopic composition of all the phases in equilibrium would vary slightly as a function of the amount of CO2 in the system produced by oxidation of graphite (Supplementary Fig. 3a), with  $\delta^{13}C_{CO2} = -10.17\%$  for  $CO_2$ /aragonite = 0 and  $\delta^{13}C_{CO2} = -11.33\%$  for  $CO_2$ /aragonite = 1. This conventional model is therefore not adequate to reproduce our experimental system, characterized by CO₂/aragonite ≈ 0.1, where both aragonite and CO<sub>2</sub> converge to much heavier compositions. However, the fit between the isotopic model and the experimental trend improves significantly (Supplementary Fig. 3a) if we assume (1) graphite as chemically reactive but isotopically inert phase and (2) starting CO<sub>2</sub> displaying  $\delta^{13}C = -20\%$ , i.e. the same value of the starting graphite. These assumptions, deduced on the basis of our experimental findings, underline again the need for experimental constraints on deep isotopic exchange processes involving fluids. For instance, an implication of our study could throw some light on the hard debate on the genesis of diamonds characterized by light, organic matterlike isotopic compositions<sup>19</sup>. In fact, even if we predict that, after having interacted at subarc conditions with graphite-saturated fluids, sedimentary carbonates will be only slightly depleted in <sup>13</sup>C, showing the same  $\delta^{13}$ C -2.8 to -3.3% characterizing CO<sub>2</sub>, they could become locally lighter (cf. brown in Fig. 4) in case of highly oxidized conditions<sup>37</sup> or very high water/carbonate (≈ fluid/rock) ratios<sup>38</sup>. Because of their stability at high-pressure conditions<sup>39</sup>, these carbonates could be subducted further, eventually making available a <sup>12</sup>C-enriched source of carbon, which comes from carbonate and not organic matter, in the diamond stability field<sup>40</sup> (Fig. 5).

The link between sedimentary slab fluids and arc emissions. As an aqueous fluid-phase species, CO2 originated from subducted sediments close to the slab-mantle interface is particularly effective in metasomatizing the subarc supra-subduction mantle, prompting carbonation reactions<sup>20,21,23,41</sup> that may facilitate diapiric upwelling and melting processes<sup>20,42</sup>. Therefore, there is good reason to believe that sediment-derived CO2 can impose its isotopic signature on the subarc mantle, the source of arc magmatism (Fig. 5). The interaction of subducted ocean carbonates and organic matter with fluids coming from the dehydration of the down-going slab<sup>25,43</sup> is a continuous process starting early in the forearc region<sup>9,44</sup> (Fig. 5; Supplementary Fig. 1). However, our study indicates that the production of CO2 is strictly connected to the stability of graphite in aqueous fluids. At forearc conditions graphite is poorly soluble by oxidative dissolution, even considering the increased dissolution susceptibility for disordered graphitic carbon, in the absence of intense flushing by aqueous fluids (i.e. channelized flow)<sup>16,36</sup>. Aqueous fluids reach their maximum CO<sub>2</sub> contents at subarc conditions (Fig. 5; Supplementary Fig. 1), which are the conditions investigated in our study<sup>16</sup>. Beneath arcs, the interaction between aqueous fluids coming from the dehydrating oceanic slab and percolating into the overlying carbonate metasediments will thus result in a large amount of CO2 leached out from the slab, as long as graphite is not completely removed by oxidative dissolution, which depends chiefly on the time-integrated fluid flux for given redox state 18. Although channelized fluid flow can potentially dissolve the entire amount of organic carbon at blueschist-to-eclogite conditions, the geological record suggests the complete removal is difficult even for very high fluxes and often limited to the more

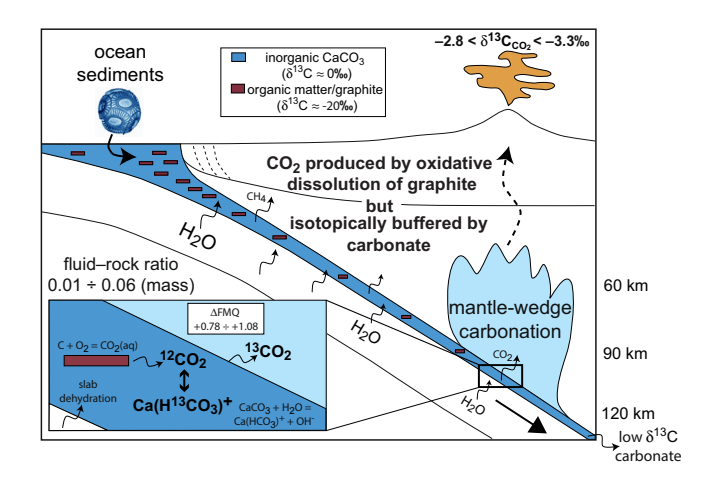


Fig. 5 Carbon isotope exchange at the subarc slab-mantle interface.

Organic (brown) and inorganic (dark blue) carbon occurring in open-ocean sediments enters the subduction channel, where it interacts with aqueous fluids produced by dehydration of the down-going oceanic lithosphere. While calcium carbonate dissolution increases almost linearly with depth<sup>14</sup>, resulting in fluids containing ~5000 ppm C mainly as Ca(HCO<sub>3</sub>)<sup>+</sup> at subarc depth, the oxidative dissolution of graphite increases exponentially and reaches its maximum at subarc conditions, where fluids coexisting with graphite contain ~140,000 ppm C mainly under the form of CO<sub>2(aq)</sub>. With the simultaneous presence of aragonite and graphite, experiments show that the carbon concentration in aqueous fluids is halved, but still controlled by oxidation of graphite to CO<sub>2</sub>. Nevertheless, as aragonite is very prone to dissolution-reprecipitation processes, it shows an outstanding capacity to buffer the isotopic signature of graphite-derived CO2 to carbonate-like values characterizing the global arc CO<sub>2</sub> (orange field). In order to exert its buffering capacity, graphite-derived CO<sub>2</sub> must be low with respect to carbonate, which is the case for low fluid-rock ratios coupled with oxidizing conditions (preferred model) or for high fluid-rock ratios coupled with relatively reducing conditions. We suggest that, as a mobile but reactive fluid-phase, CO2 is particularly effective in metasomatizing the suprasubduction mantle (light blue field), eventually imposing its isotopic signature to the deep source of arc magmatism.

soluble disordered forms of organic carbon<sup>18</sup>. Fully crystalline graphite, which is characterized by sluggish rates of isotopic diffusion<sup>3</sup>, is thus expected to persist at subarc depths. We demonstrated experimentally that the organic carbon content is not a relevant variable in controlling the carbon isotopic signature of CO<sub>2</sub> produced by dissolution processes, which only depends on redox conditions and fluid-rock ratios. Therefore,  $\delta^{13}$ C of gaseous arc emissions is not a simple linear combination of the amount of buried organic and inorganic carbon<sup>4</sup>. One major implication is that fluctuations in  $\delta^{\bar{1}3}C_{CO2}$  do not necessarily reflect variations in the source input, for instance, due to shallow crustal carbonate assimilation 45,46 or to the burial of anoxic sediments dominated by organic matter<sup>19</sup>. It could reflect instead local variations in fluid-rock ratios (i.e. channelized vs. percolating flux) or in the redox state (i.e. oxidizing vs reducing conditions). Equation 7 can be used to constrain the average redox state (expressed as  $\Delta FMQ$ ) in the sedimentary carbon source of the slab that meets the global arc  $\delta^{13}C_{CO2}$ .  $\Delta FMQ$  values ranging from +0.78 to +1.08 are predicted assuming a fluid-rock mass ratio ( $\approx$ WAR) of 0.01–0.06 (=0.05–0.33 molar), which has been suggested for infiltrating, non-channelized fluids produced by dehydration reactions in eclogites 47,48. These oxygen fugacity values are in agreement with estimations of island-arc-basalt (IAB) sources<sup>49,50</sup> and supra-subduction mantle peridotites

equilibrated at subarc depths<sup>51</sup>. It remains an open question how these oxygen fugacity values correlate with the amount of oxygen<sup>37</sup> transferred from the slab to the IAB source, with consequences for the redox budget of subarc mantle<sup>52</sup>.

#### Method

Experimental approach and characterization of the solid- and fluid phases. In this study, we employed as starting materials: (i) labelled Ca<sup>13</sup>CO<sub>3</sub> (calcite; forming aragonite at run conditions) (Sigma-Aldrich); (ii) synthetic graphite (Sigma-Aldrich), highly ordered as suggested by Raman spectroscopy<sup>16</sup>; (iii) oxalic acid di-hydrate (Sigma); (iv) MilliQ water, boiled while flushed with N2 to remove dissolved atmospheric CO2. Experiments were buffered using the double-capsule technique<sup>53</sup> (Supplementary Fig. 4) with an inner H<sub>2</sub>-permeable Au<sub>60</sub>Pd<sub>40</sub> capsule, containing the starting materials with the addition of water (~20 wt%), and an outer Au capsule filled with the buffering assemblage fayalite + magnetite + quartz + H2O (FMQ; forming ferrosilite + magnetite + coesite at run conditions, verified by electron microscopy, electron microprobe analysis and Raman spectroscopy; Supplementary Fig. 5). The buffer in the outer capsule constrains directly the  $fH_2$  in the inner capsule. The redox conditions ( $fO_2$ ) in the inner capsules are constrained indirectly by the buffer, whose  $\Delta$ FMQ is  $+0.76 \log$  units in the outer capsule, to slightly lower  $fO_2$  values ( $\Delta FMQ = +0.61$  log units; see "Thermodynamic modelling" and Supplementary Table 4).

Experiments were performed at 3 GPa and 700 °C using an end-loaded piston-cylinder apparatus. Temperatures were measured with K-type thermocouples and considered accurate to  $\pm 5$  °C. Pressure calibration is based on the quartz/coesite transition  $^{54}$  and accurate to  $\pm 0.01$  GPa. Runs with CaCO $_3$  were first pressurized at 3 GPa for 2 h, to promote carbonate crystal growth by cold sintering  $^{55}$  in order to increase the grain size of the synthetic micrometric CaCO $_3$  power. Samples are then heated to 700 °C with a ramp of 100 °C/min. Run durations were from 2.4 to 240 h. Quench is obtained by cutting off the power supply, resulting in a temperature decline of 540 °C per second. CO $_2$  water and other volatiles in the inner capsules were measured quantitatively by quadrupole mass spectrometry (QMS) using the capsule-piercing technique  $^{32}$ . The typical analytical uncertainty is 1 mol% for CO $_2$  and H $_2$ O. Solid phases were checked by scanning electron microscopy, electron microprobe analyses and micro-Raman spectroscopy.

**Isotopic analysis of CO2**. The quantitative analysis and the determination of the  $^{13}\text{C}/^{12}\text{C}$  ratio of CO2 have been performed simultaneously by means of QMS $^{32}$ , monitoring the m/z channel 45 ( $^{13}\text{CO}_2$ ) in addition to channels considered for routine analysis. The calibration curve linking the  $^{13}\text{C}/^{12}\text{C}$  ratio of CO2 and the ratio of the integrated peaks of channels 45 ( $^{13}\text{CO}_2$ ) and 44 ( $^{12}\text{CO}_2$ ) (44/45 ratio) has been derived by measuring 3 different mixtures with known  $^{13}\text{C}/^{12}\text{C}$  ratio prepared to start from (i) regular oxalic acid di-hydrate (OAD; Sigma–Aldrich), used also for OAD + Ca $^{13}\text{CO}_3$  experiments and (ii) isotopically nearly pure  $^{13}\text{C}$  oxalic acid di-hydrate (Sigma–Aldrich), thermally decomposed to CO2 at 250 °C $^{32}$  (Supplementary Table 8). Analyses performed by QMS are affected by a very small mass-bias effect. Actually, the regression line provided a very low correction factor of 1.03 for the integrated peak of channel 45.

**Isotopic analysis of solids: NanoSIMS.** <sup>13</sup>C/<sup>12</sup>C ratios of carbonate and graphite grains in the experimental sample were determined by nanoscale secondary ion mass spectrometry (NanoSIMS). Measurements were conducted on the Cameca NanoSIMS 50 installed at Muséum National d'Histoire Naturelle of Paris. The sample capsule was included in pure indium and gold-coated (20 nm thick). Secondary ions of <sup>12</sup>C<sup>12</sup>C<sup>-</sup> and <sup>13</sup>C<sup>12</sup>C<sup>-</sup> were collected in multicollection mode to obtain <sup>13</sup>C/<sup>12</sup>C ratios after calibrating with natural abundance graphite and calcite samples. 16O- secondary ions were used to locate graphite versus carbonate grains. Mass resolving power was set at a minimum 10,000, enough to resolve interferences on measured secondary ions. Before each analysis, a 5 × 5 μm<sup>2</sup> surface area was initially pre-sputtered for 60 s with a 500 pA primary Cs<sup>+</sup> rastering beam, in order to remove the gold coating and reach a sputtering steady-state<sup>56</sup>. For analyses of graphite grains, the primary beam was set to 1 pA and is was scanned over a surface area of  $5 \times 5 \,\mu\text{m}^2$ . Nevertheless, to avoid surface contamination, only ions from the inner 2.6 × 2.6 μm<sup>2</sup> regions were collected with the "beam blanking mode". Each analysis consisted of a stack of 100 cycles, with a duration of 2.048 s each. Similar settings were used to carbonate grains, except that the primary beam was set to 9 pA and each cycle was 8.192 s long. <sup>13</sup>C/<sup>12</sup>C of carbonate grains were also investigated using <sup>12</sup>C<sup>-</sup> and <sup>13</sup>C<sup>-</sup> secondary ions (mass resolving power set to 9000), showing no significant deviation from the measurements using C2- secondary ions. Due to large isotopic variations observed in these samples, instrumental mass fractionation (of a few per mil) was neglected.

**Isotopic analysis of solids: LA-ICP-MS.**  $^{13}\text{C}/^{12}\text{C}$  ratios of carbonate and graphite grains in the experimental sample were also determined by LA-ICP-MS. Measurements were carried out over a New Wave UP 266 laser ablation system coupled with a Thermo Fisher ICAP-Q ICP-MS. In order to find the best compromise between ablated surface and sensitivity, ablation conditions were optimized over a natural abundance calcite sample with a known  $^{12}\text{C}/^{13}\text{C}$  ratio (see Section "Isotopic

analysis of solids: Bulk analyses"). As a result, for each spot determination, 20 shots within 1 s were performed, using a 30 µm diameter circular spot size and adjusting the laser power to obtain a fluence value of around 17 J/cm<sup>2</sup>. Helium was used as the carrier gas (0.85 L/min). Under these conditions the hole depth (subsequently evaluated by scanning electron microscopy) is, on average, about 20 µm. Analytical accuracies and uncertainties have been evaluated by measuring the following internal standards: (i) natural abundance calcite, characterized isotopically by GasBench isotope ratio mass spectometer (IRMS) in two different laboratories (Florence and Milan), displaying an average <sup>13</sup>C abundance of 1.1208(2) %; (ii) synthetic labelled CaCO<sub>3</sub> produced by precipitation from a Na<sub>2</sub><sup>13</sup>CO<sub>3</sub> + Na<sub>2</sub><sup>12</sup>CO<sub>3</sub> solution treated with CaCl<sub>2</sub>, with <sup>13</sup>C abundance of 43.8% measured by HCl dissolution followed by QMS analysis of evolved CO2 (see "Bulk analyses" below). LA-ICP-MS measurements on these standards have been proven to be accurate to ~2% for natural calcite (standard deviation 5.8%) and ~1% for synthetic <sup>13</sup>C-<sup>12</sup>C calcite (standard deviation 0.7%) (Supplementary Table 9). Analyses of graphite are affected by a higher standard deviation of about 12%, due to decreased ablation efficiency.

Isotopic analysis of solids: Bulk analyses. Bulk analyses of the carbonates contained in the experimental capsules have been carried out by HCl decomposition followed by QMS analysis of evolved  $CO_2$  (see "Isotopic analysis of  $CO_2$ "). To perform this analysis sample capsules coming from LA-ICP-MS determination were placed in a U-shaped glass tube located upstream with respect to the QMS analyser. After 5 outgassing cycles with Ar, 1 mL of HCl (4.5 M) was introduced (from an additional port) in the bottom of the U-tube, where the capsule is located. The tube was then closed (by means of a bypass valve of the gas manifold) for 30 min in order to allow the complete decomposition of all carbonates: after this reaction time the tube was then placed in line with the QMS analyser to determine the composition of evolved  $CO_2$ . The analysis of the natural calcite standard provided a  $^{13}$ C abundance of 1.13%, which is accurate to 0.8% of the certified value. In addition, this method allowed to retrieve the  $^{13}$ C abundance of the synthesized  $^{13}$ C- $^{12}$ C calcite (43.8%) and of  $Ca^{13}$ CO<sub>3</sub> used as starting material (99.4%) (Supplementary Table 10).

The isotopic characterization of the graphite used as starting material has been performed using EA-IRMS analysis, which yielded a value of 1.0948(2)% <sup>13</sup>C.

**Thermodynamic modelling of fluid composition**. To retrieve the redox conditions in the double-capsule system, oxygen and hydrogen fugacities have been calculated by conventional thermodynamic modelling (Supplementary Table 4). In the outer capsule, containing the buffering assemblage ferrrosilite + magnetite + coesite,  $\log fO_2 = -13.21$  and  $\log fH_2 = 2.195$  have been calculated at P-T conditions of 3 GPa and 700 °C using the Perple\_X package<sup>30</sup>, considering the thermodynamic dataset of Holland and Powell<sup>57</sup> revised by the authors in 2004 (hp04ver.dat) and the equation of state "H-O HSMRK/MRK hybrid of the routine "fluids". Then,  $XCO_2 [=CO_2/(H_2O+CO_2)_{molar}] = 0.303$  for graphite-saturated fluids has been calculated by fixing  $\log fH_2 = 2.195$ , which is homogeneous in the inner and the outer capsule, using the Perplex the equation of state of Connolly and Cesare<sup>29</sup> (cf. refs. <sup>15,16</sup> for other details). This  $XCO_2$  corresponds to an innercapsule  $\log fO_2 = -13.36$  ( $\Delta FMQ = +0.61$   $\log$  units), which reflects the redox conditions occurring in the runs bearing graphite. Log  $fH_2 = 2.195$  has also been used to calculate the fluid speciation and the pH in our experimental systems, using the Deep Earth Water (DEW) model<sup>26,27</sup> (Supplementary Table 3).

**Conventional isotopic modelling.** The global  $\delta^{13}$ C of the investigated system can be expressed with the following mass balance:

$$\delta^{13}C_{\rm global} = m_{\rm graphite} \times \delta^{13}C_{\rm graphite\_\it{i}} + m_{\rm aragonite} \times \delta^{13}C_{\rm aragonite\_\it{i}}, \tag{8}$$

where m represents the molar fractions, and  $\delta^{13}C_{\text{graphite}\_i}$  and  $\delta^{13}C_{\text{aragonite}\_i}$  the initial composition of graphite and aragonite, respectively, -20% and 0% in our isotopic model.

Assuming that  $CO_2$  is produced only through oxidation of graphite (graphite\_ox), and that equilibrium conditions occur between  $CO_2$  and graphite, the isotopic composition of graphite\_ox is:

$$\delta^{13}C_{\text{graphite}\_ox} = (1 - f) \times (\delta^{13}C_{\text{graphite}\_i} - \Delta_{\text{CO},-\text{graphite}}) + f \times \delta^{13}C_{\text{graphite}\_i}$$
(9)

where  $\Delta_{\rm CO_2}$ -graphite is the CO<sub>2</sub>-graphite equilibrium fractionation factor at 700 °C<sup>58</sup> and f is the molar fraction of oxidated graphite, i.e.  $(m_{\rm graphite}-m_{\rm CO2})/m_{\rm graphite}$ , ranging from 1 (no CO<sub>2</sub> produced) to 0 (graphite fully oxidated to CO<sub>2</sub>). The isotopic composition of CO<sub>2</sub> produced by graphite oxidation is:

$$\delta^{13}C_{\text{CO}_2} = \delta^{13}C_{\text{graphite\_ox}} + \Delta_{\text{CO}_2-\text{graphite}}, \tag{10}$$

so that the lobal  $\delta^{13}C$  including  $CO_2$   $(\delta^{13}C_{global\_ox}),$  which in a closed system is numerically identical to  $\delta^{13}C_{global}$  can be expressed as:

$$\delta^{13}C_{\text{global\_ox}} = (m_{\text{graphite}} - m_{\text{CO}_2}) \times \delta^{13}C_{\text{graphite\_ox}} + m_{\text{CO}_2} \times \delta^{13}C_{\text{CO}_2} + m_{\text{aragonite}} \times \delta^{13}C_{\text{aragonite\_i}},$$
(11)

Assuming isotopic equilibrium between CO<sub>2</sub>, graphite\_ox and aragonite (Supplementary Fig. 3a), the final compositions are:

$$\delta^{13}C_{\text{aragonite}\_f} = \delta^{13}C_{\text{global\_ox}} - (m_{\text{graphite}} - m_{\text{CO}_2}) \times -\Delta_{\text{aragonite}\_\text{graphite}}) - (m_{\text{CO}_2} \times -\Delta_{\text{aragonite}\_\text{CO}_2});$$
(12)

$$\delta^{13}C_{\text{graphite\_f}} = \delta^{13}C_{\text{aragonite\_f}} - \Delta_{\text{aragonite-graphite}}; \tag{13}$$

$$\delta^{13}C_{\text{CO},f} = \delta^{13}C_{\text{aragonite},f} - \Delta_{\text{aragonite}-\text{CO},}, \tag{14}$$

In calculations considering graphite as isotopically inert (Supplementary Fig. 3b), we assume that  $CO_2$  is produced by the oxidation of graphite, but that  $CO_2$  does not equilibrate with graphite getting oxidized.

Therefore, only CO<sub>2</sub> and aragonite are freely exchanging isotopes. In this case,  $m_{\rm graphite}$  becomes 0 and  $\delta^{13}C_{\rm CO2}$  displays the constant value of –20‰. Therefore, the following equations were used instead:

$$\delta^{13}C_{global} = m_{CO2} \times 20\% + m_{Aragonite} \times \delta^{13}C_{aragonite \perp i}; \tag{15}$$

$$\delta^{13}C_{\text{aragonite}\_f} = \delta^{13}C_{\text{global}} - (m_{\text{CO2}} \times \Delta_{\text{aragonite}-\text{CO}_2}); \tag{16}$$

$$\delta^{13}C_{\text{CO}_2,f} = \delta^{13}C_{\text{aragonite},f} - \Delta_{\text{aragonite}-\text{CO}_2}.$$
 (17)

#### Data availability

The authors declare that the data supporting the findings of this study are available within the article.

#### Code availability

The authors declare that the codes developed for this study are available within the

Received: 20 May 2021; Accepted: 28 April 2022; Published online: xx xxx 2022

#### References

- Burdige, D. J. Geochemistry of Marine Sediments. (Princeton University Press, 2006).
- De Lange, G. J. et al. In Carbon Cycling In the Glacial Ocean: Constraints on the Ocean's Role in Global Change 225–258 (Springer Berlin Heidelberg, 1994).
- Kitchen, N. E. & Valley, J. W. Carbon isotope thermometry in marbles of the Adirondack Mountains, New York. J. Metamorph. Geol. 13, 577–594 (1995).
- Mason, E., Edmonds, M. & Turchyn, A. V. Remobilization of crustal carbon may dominate volcanic arc emissions. Science 357, 290–294 (2017).
- Des Marais, D. J. In Stable Isotope Geochemistry, vol. 43, 555–578 (De Gruyter Mouton, 2019).
- Valley, J. W. Stable isotope thermometry at high temperatures. Rev. Mineral. Geochem. 43, 365–413 (2001).
- Barrenechea, J. F. et al. Graphite morphologies from the Borrowdale deposit (NW England, UK): Raman and SIMS data. Contrib. Mineral. Petrol. 158, 37–51 (2009).
- Valley, J. W. & O'Neil, J. R. 13C12C exchange between calcite and graphite: a possible thermometer in Grenville marbles. *Geochim. Cosmochim. Acta* 45, 411–419 (1981).
- Gorman, P. J., Kerrick, D. M. & Connolly, J. a D. Modeling open system metamorphic decarbonation of subducting slabs. *Geochem. Geophys. Geosyst.* 7, (2006)
- Galvez, M. E. et al. Graphite formation by carbonate reduction during subduction. Nat. Geosci. 6, 473–477 (2013).
- Caciagli, N. C. & Manning, C. E. The solubility of calcite in water at 6-16 kbar and 500-800 °C. Contrib. Mineral. Petrol. 146, 275-285 (2003).
- Pan, D., Spanu, L., Harrison, B., Sverjensky, D. A. & Galli, G. Dielectric properties of water under extreme conditions and transport of carbonates in the deep Earth. *Proc. Natl Acad. Sci. USA* 110, 6646–6650 (2013).
- Facq, S., Daniel, I., Montagnac, G., Cardon, H. & Sverjensky, D. A. In situ Raman study and thermodynamic model of aqueous carbonate speciation in equilibrium with aragonite under subduction zone conditions. *Geochim. Cosmochim. Acta* 132, 375–390 (2014).
- Kelemen, P. B. & Manning, C. E. Reevaluating carbon fluxes in subduction zones, what goes down, mostly comes up. *Proc. Natl Acad. Sci. USA* https://doi.org/10.1073/pnas.1507889112 (2015).

- Tumiati, S. et al. Silicate dissolution boosts the CO<sub>2</sub> concentrations in subduction fluids. Nat. Commun. 8, 616 (2017).
- Tumiati, S. et al. Dissolution susceptibility of glass-like carbon versus crystalline graphite in high-pressure aqueous fluids and implications for the behavior of organic matter in subduction zones. *Geochim. Cosmochim. Acta* 273, 383–402 (2020).
- Ague, J. J. & Nicolescu, S. Carbon dioxide released from subduction zones by fluid-mediated reactions. Nat. Geosci. 7, 2–7 (2014).
- Vitale Brovarone, A. et al. Fluid-mediated selective dissolution of subducting carbonaceous material: Implications for carbon recycling and fluid fluxes at forearc depths. Chem. Geol. 549, (2020).
- 19. Plank, T. & Manning, C. E. Subducting carbon. Nature 574, 343-352 (2019).
- Tumiati, S., Fumagalli, P., Tiraboschi, C. & Poli, S. An experimental study on COH-bearing peridotite up to 3??2 GPa and implications for crust-mantle recycling. J. Pet. 54, 453–479 (2013).
- Sieber, M. J., Hermann, J. & Yaxley, G. M. An experimental investigation of C-O-H fluid-driven carbonation of serpentinites under forearc conditions. Earth Planet. Sci. Lett. 496, 178-188 (2018).
- Scambelluri, M. et al. Carbonation of subduction-zone serpentinite (highpressure ophicarbonate; Ligurian Western Alps) and implications for the deep carbon cycling. *Earth Planet. Sci. Lett.* 441, 155–166 (2016).
- Piccoli, F. et al. Carbonation by fluid-rock interactions at high-pressure conditions: Implications for carbon cycling in subduction zones. *Earth Planet.* Sci. Lett. 445, 146–159 (2016).
- 24. Morse, J. W. & Mackenzie, F. T. Geochemistry of Sedimentary Carbonates (Elsevier, 1990).
- Schmidt, M. W. & Poli, S. in Treatise Geochemistry, 2nd edn., vol. 4, 669–701 (2013).

Q10

Q11

Q12

- Sverjensky, D. A., Harrison, B. & Azzolini, D. Water in the deep Earth: the dielectric constant and the solubilities of quartz and corundum to 60kb and 1200 °C. Geochim. Cosmochim. Acta 129, 125–145 (2014).
- Sverjensky, D. A. Thermodynamic modelling of fluids from surficial to mantle conditions. *J. Geol. Soc. Lond.* 176, 348–374 (2019).
- Huang, F. & Sverjensky, D. A. Extended Deep Earth Water Model for predicting major element mantle metasomatism. *Geochim. Cosmochim. Acta* 254, 192–230 (2019).
- Connolly, J. A. D. & Cesare, B. C-O-H-S fluid composition and oxygen fugacity in graphitic metapelites. J. Metamorph. Geol. 11, 379–388 (1993).
- Connolly, J. A. D. Computation of phase equilibria by linear programming: a tool for geodynamic modeling and its application to subduction zone decarbonation. *Earth Planet. Sci. Lett.* 236, 524–541 (2005).
- McCollom, T. M. & Seewald, J. S. A reassessment of the potential for reduction of dissolved CO<sub>2</sub> to hydrocarbons during serpentinization of olivine. Geochim. Cosmochim. Acta 65, 3769–3778 (2001).
- 32. Tiraboschi, C., Tumiati, S., Recchia, S., Miozzi, F. & Poli, S. Quantitative analysis of COH fluids synthesized at HP–HT conditions: an optimized methodology to measure volatiles in experimental capsules. *Geofluids* 16, 841–855 (2016).
- Thrower, P. A. & Mayer, R. M. Point defects and self-diffusion in graphite. *Phys. Status Solidi a* 47, 11–37 (1978).
- Kueter, N., Schmidt, M. W., Lilley, M. D. & Bernasconi, S. M. Experimental determination of equilibrium CH4–CO2-CO carbon isotope fractionation factors (300–1200 °C). Earth Planet. Sci. Lett. 506, 64–75 (2019).
- Miozzi, F. & Tumiati, S. Aqueous concentration of CO<sub>2</sub> in carbon-saturated fluids as a highly sensitive oxybarometer. Geochem. Perspect. Lett. 16, (2021).
- Tumiati, S. & Malaspina, N. Redox processes and the role of carbon-bearing volatiles rom the slab-mantle interface to the mantle wedge. J. Geol. Soc. Lond. 176, 388–397 (2019).
- Tumiati, S., Godard, G., Martin, S., Malaspina, N. & Poli, S. Ultra-oxidized rocks in subduction mélanges? Decoupling between oxygen fugacity and oxygen availability in a Mn-rich metasomatic environment. *Lithos* 226, (2015).
- John, T., Scherer, E. E., Haase, K. & Schenk, V. Trace element fractionation during fluid-induced eclogitization in a subducting slab: Trace element and Lu-Hf-Sm-Nd isotope systematics. *Earth Planet. Sci. Lett.* 227, 441–456 (2004).
- Schettino, E. & Poli, S. In Carbon in Earth's Interior, Geophysical Monograph 249 (eds. Manning, C. E., Lin, J.-F. & Mao, W. L.) 209–221 (John Wiley & Sons, Inc., 2020).
- 40. Bureau, H., Remusat, L., Esteve, I., Pinti, D. L. & Cartigny, P. The growth of lithospheric diamonds. *Sci. Adv.* 4, 1–6 (2018).
- Tiraboschi, C. et al. Experimental determination of magnesia and silica solubilities in graphite-saturated and redox-buffered high-pressure COH fluids in equilibrium with forsterite + enstatite and magnesite + enstatite. Contrib. Mineral. Petrol. 173, 2 (2018).
- Marschall, H. R. & Schumacher, J. C. Arc magmas sourced from mélange diapirs in subduction zones. Nat. Geosci. 5, 862–867 (2012).

- Pellegrino, L., Malaspina, N., Zanchetta, S., Langone, A. & Tumiati, S. High pressure melting of eclogites and metasomatism of garnet peridotites from Monte Duria Area (Central Alps, N Italy): a proxy for melt-rock reaction during subduction. *Lithos* 358–359 (2020).
- Piccoli, F., Ague, J. J., Chu, X., Tian, M. & Vitale Brovarone, A. Field-based evidence for intra-slab high-permeability channel formation at eclogite-facies conditions during subduction. *Geochem. Geophys. Geosyst.* 22, 1–17 (2021).
- Troll, V. R. et al. Crustal CO<sub>2</sub> liberation during the 2006 eruption and earthquake events at Merapi volcano, Indonesia. *Geophys. Res. Lett.* 39, 1–6 (2012).
- Freda, C. et al. CO<sub>2</sub>-driven large mafic explosive eruptions: the Pozzolane Rosse case study from the Colli Albani Volcanic District (Italy). *Bull. Volcanol.* 73, 241–256 (2011).
- Marschall, H. R., Pogge von Strandmann, P. A. E., Seitz, H. M., Elliott, T. & Niu, Y. The lithium isotopic composition of orogenic eclogites and deep subducted slabs. *Earth Planet. Sci. Lett.* 262, 563–580 (2007).
- Konrad-Schmolke, M., Zack, T., O'Brien, P. J. & Barth, M. Fluid migration above a subducted slab - Thermodynamic and trace element modelling of fluid-rock interaction in partially overprinted eclogite-facies rocks (Sesia Zone, Western Alps). Earth Planet. Sci. Lett. 311, 287–298 (2011).
- Mallmann, G. & O'Neill, H. S. C. The crystal/melt partitioning of V during mantle melting as a function of oxygen fugacity compared with some other elements (Al, P, Ca, Sc, Ti, Cr, Fe, Ga, Y, Zr and Nb). J. Pet. 50, 1765–1794 (2009).
- Parkinson, I. J. & Arculus, R. J. The redox state of subduction zones: insights from arc-peridotites. Chem. Geol. 160, 409–423 (1999).
- Cannaò, É. & Malaspina, N. From oceanic to continental subduction: implications for the geochemical and redox evolution of the supra-subduction mantle. 14, (2018).
- Evans, K. A., Elburg, M. A. & Kamenetsky, V. S. Oxidation state of subarc mantle. Geology 40, 783–786 (2012).
- Eugster, H. P. & Skippen, G. B. Igneous and metamorphic reactions involving gas equilibria. Res. Geochem. 2, 492–520 (1967).
- Bose, K. & Ganguly, J. Quartz-coesite transition revisited; reversed experimental determination at 500-1200 degrees C and retrieved thermochemical properties. Am. Mineral. 80, 231–238 (1995).
- De Silva, P., Bucea, L., Sirivivatnanon, V. & Moorehead, D. R. Carbonate binders by 'cold sintering' of calcium carbonate. J. Mater. Sci. 42, 6792–6797 (2007).
- Thomen, A., Robert, F. & Remusat, L. Determination of the nitrogen abundance in organic materials by NanoSIMS quantitative imaging. *J. Anal. Atomic Spectrom.* 29, 512–519 (2014).
- 57. Holland, T. J. B. & Powell, R. An internally consistent thermodynamic data set for phases pf petrological interest. *J. Metamorph. Geol.* **16**, 309–343 (1998).
- Bottinga, Y. Calculated fractionation factors for carbon and hydrogen isotope exchange in the system. *Geochim. Cosmochim. Acta* 33, 49–64 (1969).

#### **Acknowledgements**

Elena Ferrari and Chiara Compostella (University of Milan) are acknowledged, respectively, for the IRMS analyses of natural abundance calcite standard, provided by Marilena Moroni (University of Milan), and of synthetic graphite used as starting material. Andrea Amalfa and Francesca Miozzi (University of Milan) helped in preparing some of the experiments. Andrea Risplendente (University of Milan) assisted to perform microprobe analysis and scanning electron microscopy. Luca Toffolo (University of Padova, Italy) and Patrizia Fumagalli (University of Milan) are acknowledged for micro-Raman spectroscopy. L.R. acknowledges the NanoSIMS facility at the Muséum National d'Histoire Naturelle in Paris, established by funds from the CNRS, Région Ile de France, Ministère délégué à l'Enseignement supérieur et à la Recherche, and the Muséum National d'Histoire Naturelle. S.T. and S.P. acknowledge support from the Italian program MIUR PRIN 2017ZE49E7 002.

#### **Author contributions**

S.T. conceived the experimental study, analyzed the experimental fluids by QMS, wrote the manuscript and is responsible for data reduction and analysis. S.R. and D.S. performed the LA-ICP-MS and the bulk carbonate analysis by QMS. L.R. carried out the NanoSIMS analysis. C.T. prepared most of the experiments. D.A.S. supervised the thermodynamic modelling of fluids. C.E.M., D.A.S. and S.P. collaborate to the final version of the manuscript. A.V.B. and A.B. performed the conventional isotopic modelling. S.P. provided funds to support this study.

#### **Competing interests**

The authors declare no competing interests.





#### **Additional information**

**Supplementary information** The online version contains supplementary material available at https://doi.org/10.1038/s41467-022-30421-5.

Correspondence and requests for materials should be addressed to S. Tumiati.

**Peer review information** *Nature Communications* thanks the anonymous reviewer(s) for their contribution to the peer review of this work. Peer reviewer reports are available.

Reprints and permission information is available at http://www.nature.com/reprints

**Publisher's note** Springer Nature remains neutral with regard to jurisdictional claims in published maps and institutional affiliations.



**Open Access** This article is licensed under a Creative Commons Attribution 4.0 International License, which permits use, sharing,

adaptation, distribution and reproduction in any medium or format, as long as you give appropriate credit to the original author(s) and the source, provide a link to the Creative Commons license, and indicate if changes were made. The images or other third party material in this article are included in the article's Creative Commons license, unless indicated otherwise in a credit line to the material. If material is not included in the article's Creative Commons license and your intended use is not permitted by statutory regulation or exceeds the permitted use, you will need to obtain permission directly from the copyright holder. To view a copy of this license, visit http://creativecommons.org/licenses/by/4.0/.

© The Author(s) 2022

# **QUERY FORM**

NATURECOMMUNICATIONS			
Manuscript ID	[Art. Id: 30421]		
Author			
Editor			
Publisher			

## Journal: NATURECOMMUNICATIONS

**Author**: The following queries have arisen during the editing of your manuscript. Please answer by making the requisite corrections directly in the e.proofing tool rather than marking them up on the PDF. This will ensure that your corrections are incorporated accurately and that your paper is published as quickly as possible.

Query No.	Description	Author's Response
AQ1	Please check your article carefully, coordinate with any co-authors and enter all final edits clearly in the eproof, remembering to save frequently. If edits are needed to figures, please attach a corrected figure file containing the relevant changes. Once corrections are submitted, we cannot routinely make further changes to the article.	
AQ2	Note that the eproof should be amended in only one browser window at any one time; otherwise changes will be overwritten.	
AQ3	Author surnames have been highlighted. Please check these carefully and adjust if the first name or surname is marked up incorrectly. Note that changes here will affect indexing of your article in public repositories such as PubMed. Also, carefully check the spelling and numbering of all author names and affiliations, and the corresponding email address(es).	
AQ4	You cannot alter accepted Supplementary Information files except for critical changes to scientific content. If you do resupply any files, please also provide a brief (but complete) list of changes. If these are not considered scientific changes, any altered Supplementary files will not be used, only the originally accepted version will be published.	
AQ5	If applicable, please ensure that any accession codes and datasets whose DOIs or other identifiers are mentioned in the paper are scheduled for public release as soon as possible, we recommend within a few days of submitting your proof, and update the database record with publication details from this article once available.	
AQ6	Reference 31 was not originally cited in text. Please confirm that the citation of this reference after the sentence 'modelling of graphite-saturated COH fluids' is ok.	

# **QUERY FORM**

NATURECOMMUNICATIONS			
Manuscript ID	[Art. Id: 30421]		
Author			
Editor			
Publisher			

## Journal: NATURECOMMUNICATIONS

**Author**: The following queries have arisen during the editing of your manuscript. Please answer by making the requisite corrections directly in the e.proofing tool rather than marking them up on the PDF. This will ensure that your corrections are incorporated accurately and that your paper is published as quickly as possible.

Query No.	Description	Author's Response
AQ7	Reference [56] is a duplicate of [32] and hence the repeated version has been deleted. Please check.	
AQ8	Please provide page range for reference 9.	
AQ9	Please provide page range for reference 18.	
AQ10	Please provide publisher's name for reference 25.	
AQ11	Please provide page range for reference 35.	
AQ12	Please provide page range for reference 37.	
AQ13	Please provide volume number for reference 43.	
AQ14	Please provide journal name and page range for reference 51.	